Supporting Information for "The path toward the vertical grid options for the Community Atmosphere Model 7: the impact of vertical resolution on the QBO and tropical waves"

Isla R. Simpson[1], Rolando R. Garcia[1], Julio T. Bacmeister[1], Peter H. Lauritzen[1], Cecile Hannay[1], Brian Medeiros[1], Julie M. Caron[1], Gokhan Danabasoglu[1], Adam Herrington[1], Christiane Jablonowski[2], Dan Marsh[1,3], Richard B. Neale[1], Lorenzo M. Polvani[4,5], Jadwiga H. Richter[1], Nan Rosenbloom[1], Simone Tilmes[2]

[1]NSF National Center for Atmospheric Research, Boulder, CO, USA

[2]Department of Climate and Space Sciences and Engineering, University of Michigan, Ann Arbor, MI, USA

[3]School of Physics and Astronomy, University of Leeds, Leeds, UK

[4]Department of Applied Physics and Applied Mathematics, Columbia University, New York, NY, USA

[5]Lamont-Doherty Earth Observatory, Columbia University, Palisades, NY, USA

Contents of this file

Text S1.

The bug that was found in the 140 km and 80 km top simulations relates to some spurious behavior of the gravity wave drag routine. The gravity wave drag routine involves a

top-down loop that calculates wind tendencies, applies limiters to prevent wind tendencies from becoming unphysical and then recomputes the momentum flux profile to be consistent with these corrected wind tendencies. This algorithm made an assumption that the magnitude of the momentum flux decreases monotonically in altitude, which is true most of the time unless floating point arithmetic produces a spurious positive gradient with increasing altitude. If such a spurious momentum flux gradient occurs, the algorithm can lead to a spurious source of drag in the troposphere. With higher vertical resolution, the conditions which lead to this spurious drag were met more frequently. As a result, it became apparent in the high resolution cases, but has much less of an impact on the climate in the low resolution cases. This bug has an impact on tropospheric climate, primarily the extra-tropical planetary wave structures. It has no detectable effect on tropical dynamics as the parameterized waves in the tropics are mainly convectively or orographically forced with a narrow range of phase velocities and relatively large source amplitudes. As a result, they all break or are absorbed mainly in the troposphere and stratosphere, such that the accumulation of errors that leads to spurious results in extratropical latitudes, where the frontally-generated gravity waves often propagate to much higher altitudes, is not present. We verify that it does not impact on the conclusions regarding the wave driving of the QBO in the dz500 case at 80 km by comparing a simulation with the bug and the simulation without the bug in Fig. S1. However, this does mean that the simulations with varying dz cannot be used to explore the impacts of resolution on the extra-tropics.

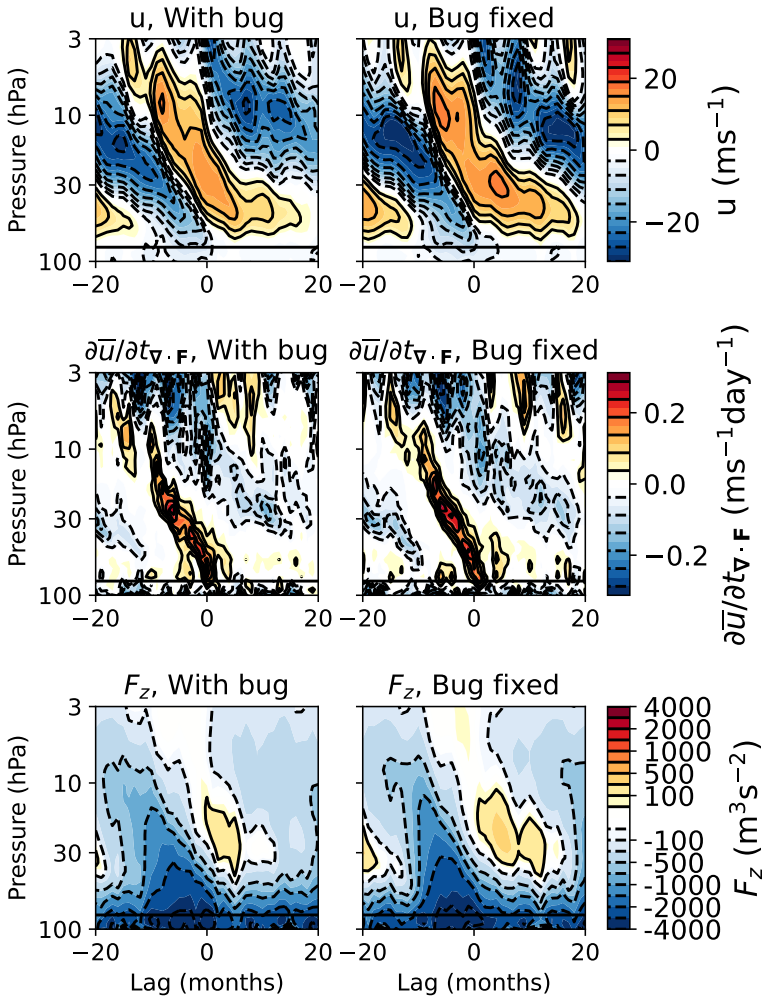

Figure S1. As Fig. 2 of the main text but comparing two simulations with dz500 and the 80 km top. The simulation on the left has the bug described in text S1 and the simulation on the right has the bug fixed. Panels show composites of monthly averaged fields area averaged from 5°S to 5°N and lagged relative to the month at which the zonal mean zonal wind area averaged from 5°S to 5°N at 50 hPa transitions from easterly to westerly. (Top) shows zonal mean zonal wind, (middle) shows zonal wind tendency due to the E-P flux divergence, (bottom) shows the vertical component of the E-P flux.

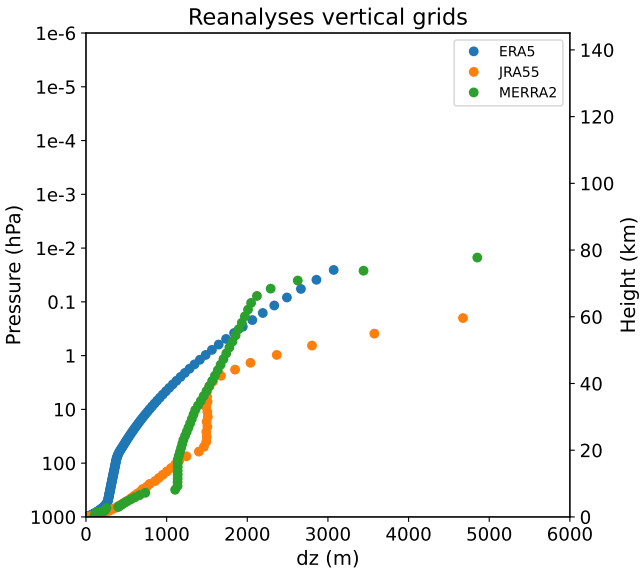

Figure S2. Vertical grid spacing of reanalysis products: ERA5 (blue), JRA55 (orange), and MERRA2 (green).

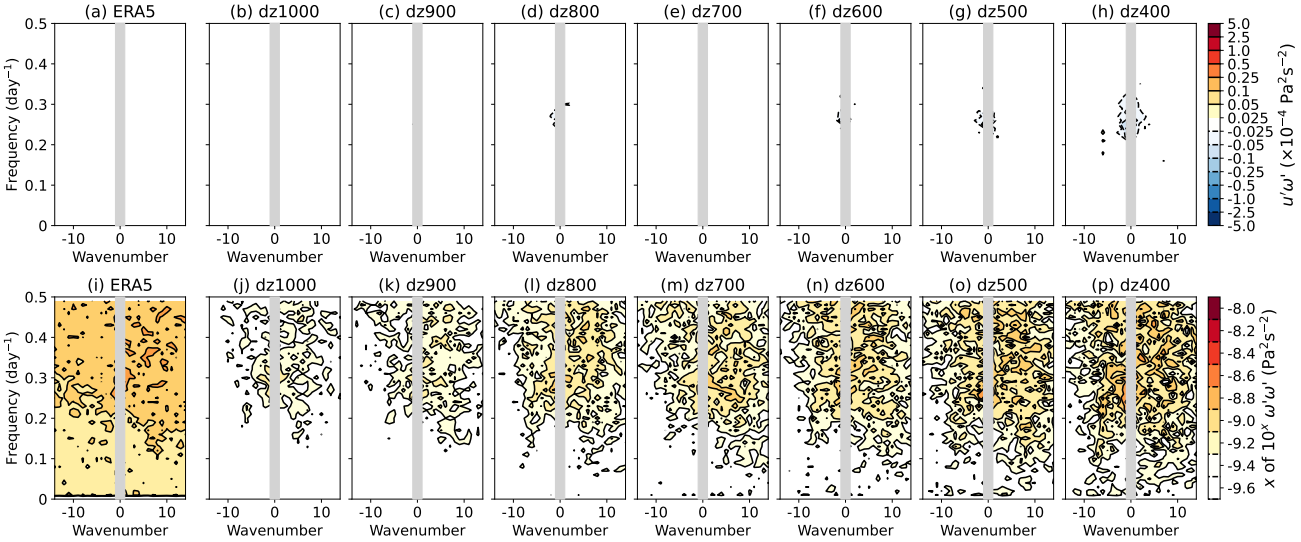

Figure S3. As Fig. 6 of the main text but for waves that are antisymmetric about the equator. (a)-(h) show the cospectra of the zonal mean vertical eddy momentum flux at 50 hPa ($\overline{u'\omega'}$) averaged over 5°S to 5°N as a flux per 0.01 day^{-1} frequency by 1 wavenumber bin, calculated over the approximately 90 days prior to the transition from easterly to westerly at 50 hPa. Note the non-linear contour interval and that the contour interval is the same as that of the equivalent plots in the main text Figure 5. (i)-(p) are as (a)-(h) but showing the power spectra of ω on a logarithmic scale. Note that here the scale is different from that in main text Figure 5 because the power in these waves is much smaller than that of the symmetric waves.

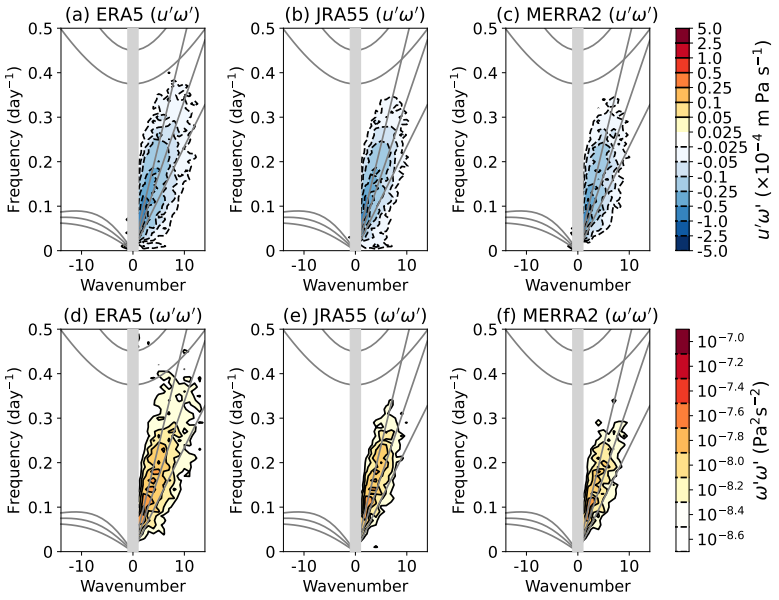

Figure S4. As Fig. 6 of the main text but for each of the reanalysis products. (top) Cospectra of the zonal mean vertical eddy momentum flux at 50 hPa ($\overline{u'\omega'}$) averaged over 5°S to 5°N for waves that are symmetric about the equator expressed as a flux per 0.01 day^{-1} frequency by 1 wavenumber bin, calculated over the approximately 90 days prior to the transition from easterly to westerly at 50 hPa. (d)-(f) are as (a)-(c) but showing the power spectra of ω on a logarithmic scale. The gray curves depict the dispersion curves for Kelvin waves, inertio-gravity waves, and equatorial Rossby waves for equivalent depths of 12, 25, and 50 m. (f)-(j) are as (a)-(e) but showing the power spectra of ω on a logarithmic scale. (left) ERA5, (middle) JRA55, and (right) MERRA2.

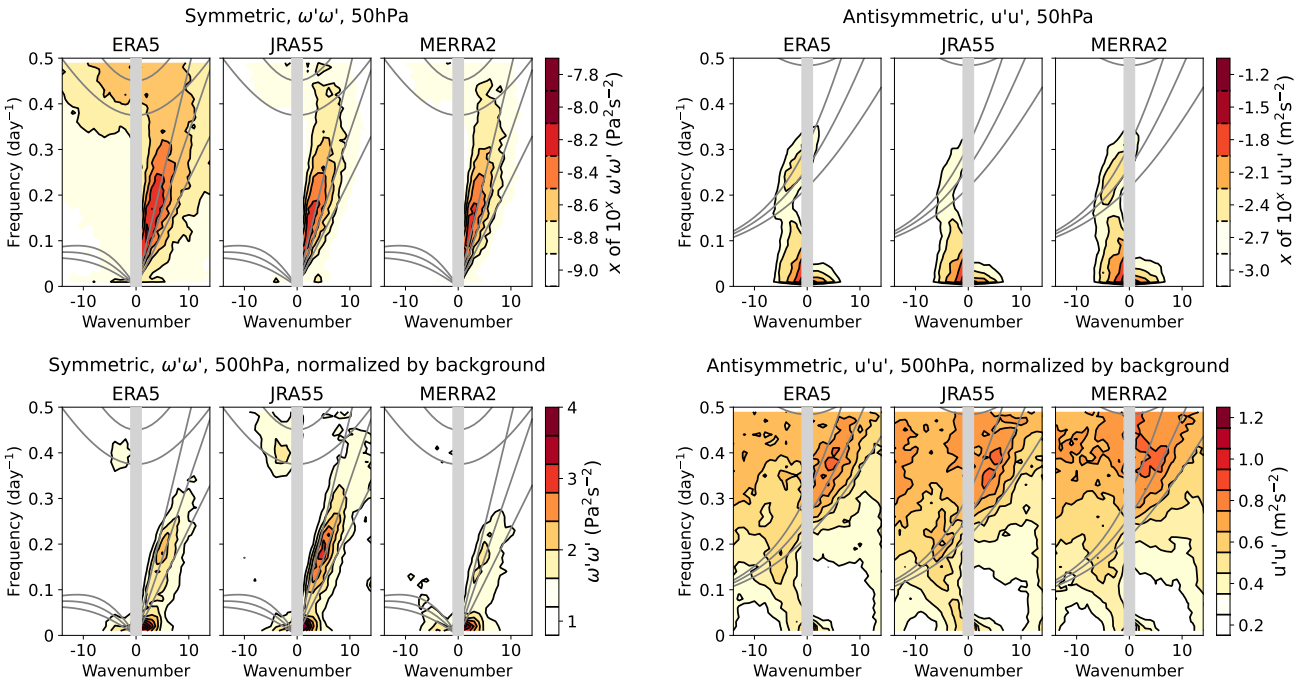

Figure S5. As Fig. 7 (left) and Fig. 8 (right) of the main text but comparing the three reanalyses. (Left) shows power spectra of eddy vertical (pressure) velocity that is symmetric about the equator averaged from 5°S to 5°N. (Top row) at 50 hPa on a logarithmic scale, and (bottom row) at 500 hPa after normalizing by the background. In the bottom row the power spectrum is smoothed with a two-dimensional Gaussian filter with a standard deviation of 1. (Right) is as left but for power spectra of the component of the eddy zonal wind that is antisymmetric about the equator averaged from 5°S to 5°N.

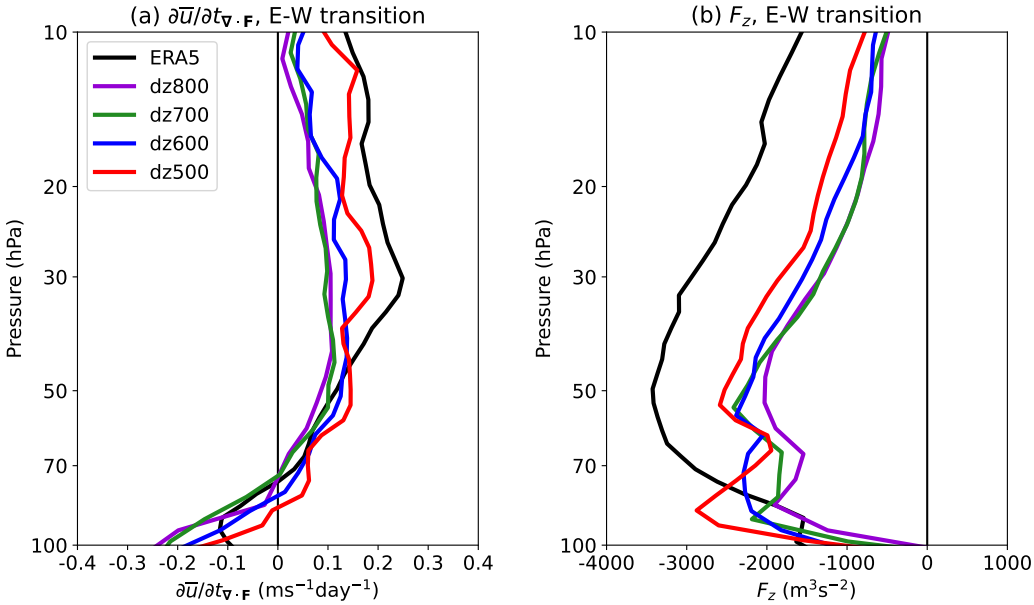

Figure S6. As Fig. 4 of the main text but with the model top at ∼80 km. (a) Composites of the zonal mean zonal wind tendency due to resolved waves for ERA5 and the 80 km top simulations for the 90 days prior to the transition from easterly to westerly determined separately for each level. (b) is as (a) but for the vertical component of the E-P flux (F_z).

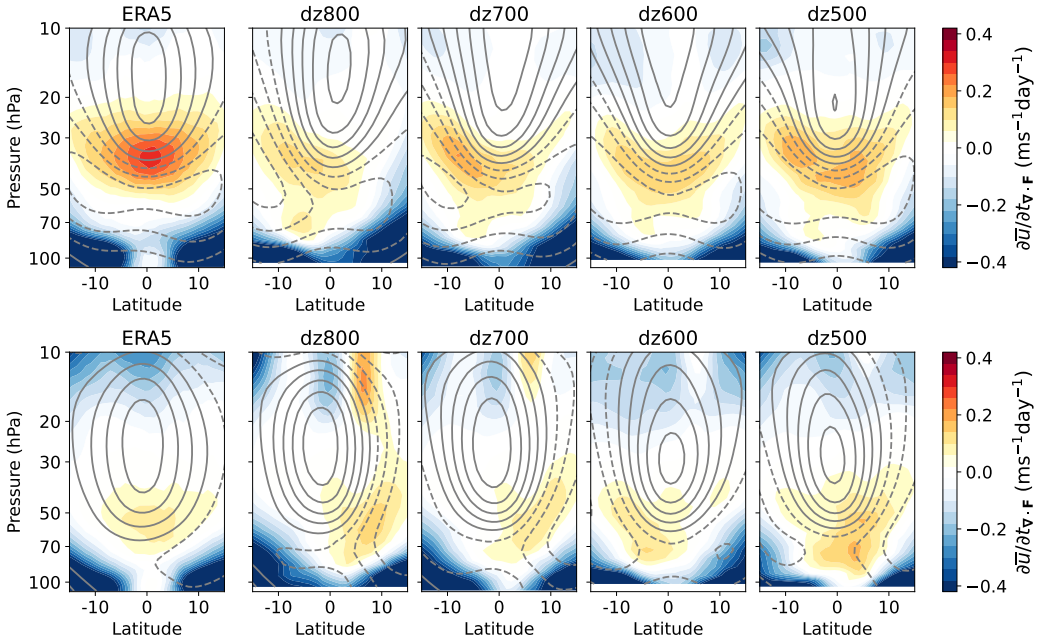

Figure S7. As Fig. 5 of the main text but for the 80 km top simulations. Latitude-Pressure cross sections of the E-P flux divergence i.e., the zonal mean zonal wind tendency due to resolved waves (in color shading) and the zonal mean zonal wind (in contours with a contour interval of 4ms^{-1} and dashed contours being negative and solid contours being zero or positive). The top panels show the composites for the 90 days prior to the transition to westerlies at 50 hPa and the bottom panels show the composites for the 90 days after the transition to westerlies at 50 hPa.

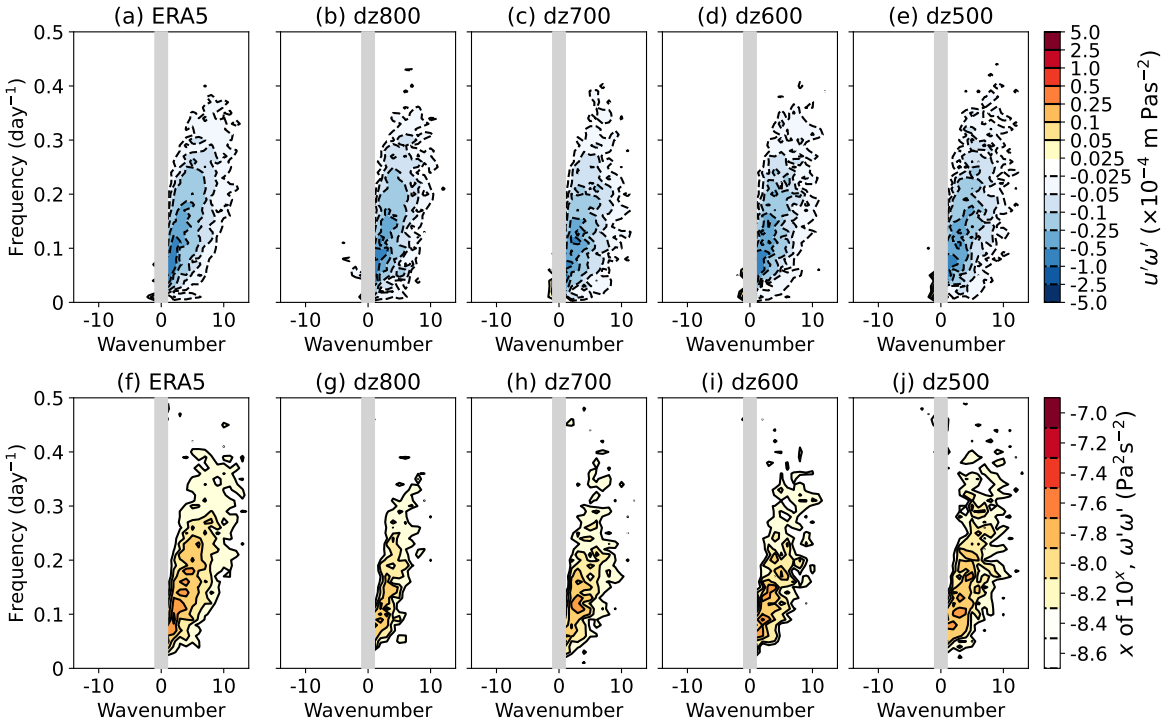

Figure S8. As Fig. 6 of the main text but for the 80 km top simulations. (a)-(e) Cospectra of the zonal mean vertical eddy momentum flux at 50 hPa ($\overline{u'\omega'}$) averaged over 5°S to 5°N for motions that are symmetric about the equator expressed as a flux per 0.01 day^{-1} frequency by 1 wavenumber bin, calculated over the approximately 90 days prior to the transition from easterly to westerly at 50 hPa with tapering applied over the first and last 5 days (see section 3.3 for the method). Left shows ERA5 and the subsequent panels from left to right show dz800, dz700, dz600, and dz500. Note the non-linear contour interval. (f)-(j) are as (a)-(e) but showing the power spectra of ω on a logarithmic scale.

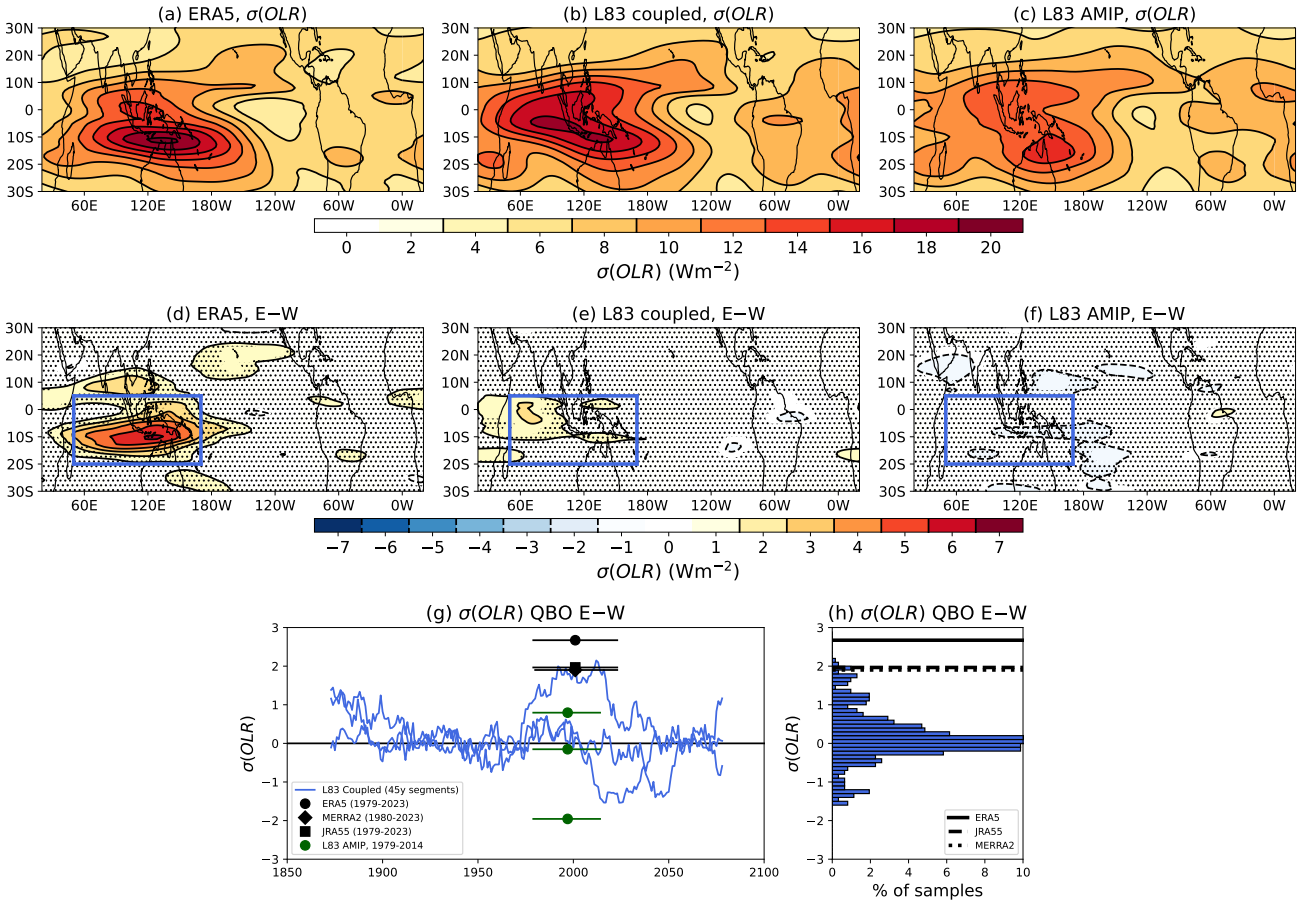

Figure S9. As Fig. 18 of the main text but using MJO filtered Outgoing Longwave Radiation (OLR). (a)-(c) the climatological standard deviation of MJO filtered OLR ($\sigma(OLR)$) computed as the standard deviation across days within the winter for each year and then averaged across years for (a) ERA5 from 1979 to 2023, (b) Coupled L83 using 1979 to 2023, (c) AMIP L83 using 1979 to 2020. (d)-(f) are as (a)-(c) but for the difference in $\sigma(OLR)$ between QBO easterly years and QBO westerly years. (g) shows the difference in $\sigma(OLR)$ between easterly and westerly QBO averaged over the blue box in panels (d)-(f) i.e., 50°W to 170°W, 20°S to 5°N. The blue line shows the values obtained using consecutive 45 year windows i.e., the same length as the 1979 to 2023 ERA5 record. The green points show the L83 AMIP simulations using the period 1979 to 2020 and the black points show the reanalyses over 1979 to 2023. (h) Shows the PDF of the difference in $\sigma(OLR)$ between QBO easterly and westerly years for all the 45 year segments shown in panel (g) along with the three reanalyses.

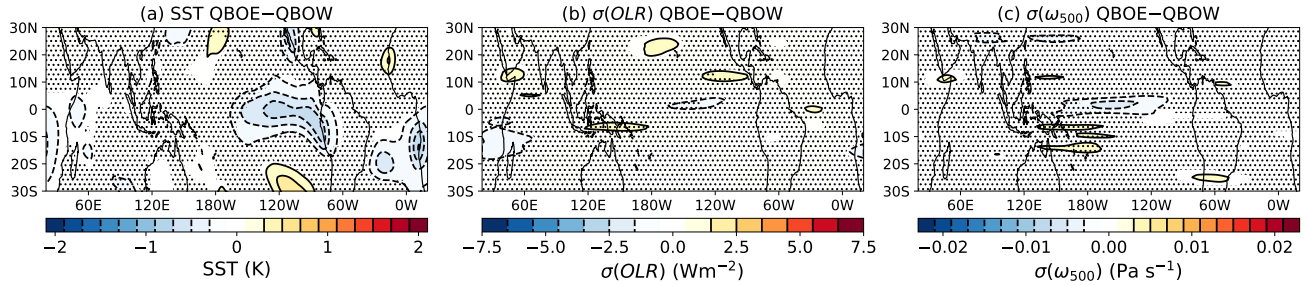

Figure S10. Composites of QBO easterly minus QBO westerly DJF seasons from the L83 AMIP simulations but with the QBO easterly and westerly years defined using the observed QBO. (a) Composite difference in SSTs, (b) composite difference in MJO filtered OLR standard deviation, (c) composite difference in MJO filtered 500 hPa vertical velocity. Stippling shows regions where the composite difference is not statistically significant at the 95% level by a bootstrapping test where the QBO easterly and westerly years from the three members are pooled together and then resampled with replacement 1000 times to produce 1000 QBO easterly minus westerly composites. Significance is determined where the 2.5th to 97.5th percentile range of these bootstrapped differences does not encompass zero.